RBRH

Revista Brasileira de Recursos Hídricos
Brazilian Journal of Water Resources
Versão On-line ISSN 2318-0331
RBRH, Porto Alegre, v. 30, e36, 2025
Scientific/Technical Article

https://doi.org/10.1590/2318-0331.302520240102

Homogeneous climate risk zones in Brazil

Zonas de risco climático homogêneo no Brasil

Carlos Eduardo Sousa Lima[1], Francisco de Assis Souza Filho[1] & Renan Vieira Rocha[2]

[1]Universidade Federal do Ceará, Fortaleza, CE, Brasil
[2]Fundação Cearense de Meteorologia e Recursos Hídricos, Fortaleza, CE, Brasil
E-mails: eduardolima@alu.ufc.br (CESL), assis@ufc.br (FASF), renan.rocha@funceme.br (RVR)

Received: September 27, 2024 - Revised: March 28, 2025 - Accepted: May 16, 2025

ABSTRACT

Brazil has a heterogeneous climate throughout its territory which makes it difficult to outline a single climate risk management strategy. However, this unification can occur within sub-regions that present homogeneous climatic risk. In this context, the aim of this study was to delineate homogeneous climate risk zones in Brazil. For this we used monthly precipitation data for the Brazilian territory provided by the Global Precipitation Climatology Center. These time series were standardized using the Standard Precipitation Index and then their homogeneous clusters were defined using the K-means method. In addition, the joint variability patterns between the clusters' centroid time series and high- and low-frequency climate variability modes were evaluated using Cross-Wavelet Analysis. The analyses carried out enabled the delineation of 7 homogeneous climate risk zones in Brazil, which showed different variability patterns and were modulated differently by the climate variability modes assessed.

Keywords: Climate risk; SPI; K-Means; Cross-wavelet analysis; Climate indices.

RESUMO

O Brasil apresenta uma heterogeneidade climática ao longo do seu território que dificulta o delineamento de uma única estratégia de gestão dos riscos climáticos. Entretanto, essa unificação pode ocorrer em sub-regiões que apresentem um risco climático homogêneo. Nesse contexto, o presente estudo objetivou o delineamento das zonas de risco climático homogêneo do Brasil. Para isso, utilizou-se dados mensais de precipitação para todo o território brasileiro fornecidos pelo *Global Precipitation Climatology Center*. Essas séries temporais foram padronizadas usando o *Standard Precipitation Index* e, em seguida, os agrupamentos homogêneos foram definidos usando o método *K-means*. Ademais, os padrões de variabilidade conjunta entre as séries temporais dos centroides desses agrupamentos e os modos de variabilidade climática de alta e baixa frequência foram avaliados por meio da análise de ondeletas cruzadas. As análises realizadas permitiram o delineamento de 7 zonas de risco climático homogêneo no Brasil, que apresentaram diferentes padrões de variabilidade e foram moduladas de forma distinta pelos modos de variabilidade climática avaliados.

Palavras-chave: Risco climático; SPI; K-Means; Ondeletas cruzadas; Índices climáticos.

INTRODUÇÃO

Anomalous atmospheric-oceanic patterns modulate weather and climate on the planet. These anomalous patterns, such as the El Niño Southern Oscillation (ENSO), develop in specific regions, remotely generating climate anomalies over an extensive region of the planet. This remote influence is called teleconnections (Reboita et al., 2021; Rocha & Souza Filho, 2020; Kayano et al., 2020; Kayano et al., 2019).

The most diverse known anomalous atmospheric-oceanic patterns are responsible for temporal fluctuations in hydrometeorological variables of diverse regions of the planet. These fluctuations are responsible for the occurrence of hydrometeorological extremes and occur on a wide range of time scales, such as: sub-seasonal, seasonal, inter-annual, decadal, multidecadal (Reboita et al., 2021; Lima et al., 2021; Grimm et al., 2020; Rocha et al., 2019).

Brazil, located on the continent of South America, is influenced by various climate variation modes due to its vast territorial extension (Reboita et al., 2010). These variation modes do not act homogeneously throughout its territory, varying the magnitude and direction of the fluctuation. Historically, several hydrometeorological extremes have been recorded in Brazil as a result of modes of climate variation induced by different anomalous atmospheric-oceanic patterns.

In the Brazilian Northeast, for example, droughts have been reported since the 16th century, accounting for huge socioeconomic losses to the region throughout their occurrences (Marengo et al., 2017, 2018). Despite the great influence of ENSO on the region's interannual climate variability, it only partially explains it, with only a few drought events being associated with this pattern of Sea Surface Temperature (SST) anomalies. Other SST anomalies can explain the occurrence of droughts that are not related to the warm phase of ENSO, e.g., the warming of the Tropical North Atlantic (TNA), which is responsible for the anomalous position of the Intertropical Convergence Zone (ITCZ) further north, affecting precipitation volumes in the region. (Marengo et al., 2017).

Technical literature also reports climatic extremes in other regions of Brazil. Coelho et al. (2016) cite the occurrences of droughts in Southeast Brazil in the austral summers of 2001 and 2014, presenting a schematic structure of the teleconnections responsible for the latter. Marengo & Espinoza (2016) point out the years in which flood and drought extremes occur in the Amazon region, located in the North of Brazil, discussing the influence of ENSO and TNA on the occurrence of these extremes. Grimm et al. (2020) discuss the combined effect the Atlantic Multidecadal Oscillation (AMO) and the Pacific Decadal Oscillation (PDO), both interdecadal climate variation modes, and the ENSO (interannual climate variation mode) on the production of climate extremes in Southern Brazil, emphasizing the 2020 drought episode and indicating past occurrences of other drought events.

The close relationship between hydrometeorological extremes and climate variation modes on different time scales imposes on water resource management the need to understand the influence of these modes, including their combined effects, for an effective climate risk management (Grimm et al., 2020; Rocha et al., 2019).

In terms of proactive climate risk management, it is essential that three steps are essential: i) monitoring and early warning, ii) identification of vulnerabilities and iii) definition and implemention of measures to mitigate the impacts of hydrometeorological extremes. In Brazil, thinking about a single proactive management model for this risk is a great challenge, as there are huge socioeconomic differences and climatic heterogeneity throughout the country, which vary the vulnerabilitiy and climate risk in its regions.

Proactive climate risk management strategies must be capable of quantifying the risks and proposing measures to mitigate their impacts (Rocha et al., 2019). In the context of climatic heterogeneity between Brazilian regions, it is interesting that such strategies are defined for regions of homogeneous climatic risk, ensuring that risk quantification and mitigation measures will be efficient throughout these areas. Definitions of homogeneous climate risk zones to improve climate risk management have been carried out in different regions of the planet, such as: East Rwanda (Sebaziga et al., 2023), Japan (Liu & Masago, 2023), Ethiopia (Tibebe et al., 2023), Ecuador (Ilbay-Yupa et al., 2021), Northeastern Argentine region (Aliaga & Piccolo, 2021) and Iberian Peninsula (Merino et al., 2015),

In Brazil, a brief technical literature review revealed that there are few studies on the delimitation and discussion of homogeneous climatic risk zones. Among the several articles that were consulted, Reboita et al. (2010) and Grimm (2011) stand out. Reboita et al. (2010) presented a literature review on precipitation regimes in South America (SA), regionalizing it into 8 sectors based on a visual analysis of the climatological precipitation graphs from various meteorological stations in the analyzed region. Similarly, Grimm (2011) discusses the interannual variability of precipitation in SA using climatological precipitation information to distinguish its different annual precipitation cycles. The authors defined the El Niño Southern Oscillation (ENSO) and the South Atlantic Convergence Zone (SACZ) as the two main modes of interannual rainfall variability in Southern SA, discussing their influence on annual and seasonal rainfall and the occurrence of extremes.

Although the abovementioned studies by Reboita et al. (2010) and Grimm (2011) differentiate between regions with different annual precipitation cycles in SA, we consider the presented regionalization to be unsatisfactory for delimiting homogeneous climatic risk zones. Because they are based only on the precipitation climatology, these regionalizations do not robustly explore the multiple characteristics of Brazilian climatic heterogeneity, for example, the different influences of the multiple climatic mechanisms responsible for climate variability in Brazil, which may operate on different time scales (Lima et al., 2021) and interact with each other, amplifying their influences (Kayano et al., 2019).

This paper proposes the delimitation of Homogeneous Climatic Risk Zones throughout Brazilian territory, attempting to correlate them with the main climate variation modes that act on different time scales. For this purpose, a clustering analysis was initially carried out considering the Standard Precipitation Index (SPI) time series of each grid point of the Global Precipitation Climate Center (GPCC) database contained in Brazilian territory. Then, a Cross Wavelet Analysis (XTC) was performed between the time series of the centroids of the delimited clusters and the time series of the Oceanic Niño Index (ONI), Pacific Decadal Oscillation (PDO) and Atlantic Multidecadal Oscillation (AMO) climate indices. In this way, in

addition to delimiting these regions with the SPI time series, it was possible to evaluate the joint variability patterns between these regions and the aforementioned climate indices, identifying the relationship between their phases.

MATERIAL AND METHODS

Figure 1 shows a graphical summary of the methodology employed in this study to determine the Brazil's homogeneous climatic risk zones. This methodology takes into account three steps:

- Step 1: Standardization of the precipitation time series using the 12-month SPI (SPI12);
- Step 2: Determination of the SPI time series clusters using the K-means algorithm;
- Step 3: Application of the XTC to identify the patterns of joint variability between the time series of the clusters' centroids and of the considered climatic indices, as well as the relationship between their phases.

Study data

Precipitation information over the Brazilian territory was obtained from the 2022 version of the global grid of monthly precipitation under the earth's surface provided by the GPCC. In this version, the rainfall grid over the earth's surface is estimated based on approximately 86,000 stations in the most diverse regions of the planet, which have at least 10 years of records. The provided historical precipitation time series covers the period between 1891 and 2020 for different grid resolutions: 0.25°, 0.5°, 1.0° and 2.5°. A grid resolution of 1° was adopted in this study (Schneider et al., 2022).

For older periods, where there is no record of precipitation in some regions or in their neighboring regions, the GPCC assigns the climatological precipitation in the period without data, ensuring that there are no anomalies between this period and the rest of the time series (Schneider et al., 2022). In order to avoid periods filled with climatological precipitation, we decided to use precipitation series from 1951 to 2020.

The main motivation for adopting the GPCC data to determine precipitation over Brazilian territory lies in the uniformity, both spatial and temporal, of the grid on which this data is made available. In addition, it is worth noting that the rainfall stations available on the National Water and Sanitation Agency's (ANA) database, called HIDROWEB, generally show discontinuities in the observed period and different lengths and periods of observation.

Furthermore, in addition to the aforementioned justifications for using the precipitation information provided by the GPCC, it is worth highlighting the studies that have evaluated the performance of this information in representing climate variability, estimating climate extremes, hydrological modeling, among other applications, such as: Kouakou et al. (2023), Dhungana et al. (2023), Santos et al. (2023), Song et al. (2022) and Gomes et al. (2022). In general, these studies classify this information as at least satisfactory.

Monthly time series of the ONI, PDO and AMO climate indices were also obtained for the period between 1951 and 2020. This information is available free of charge from the National Oceanic and Atmospheric Admnistration (NOOA) at the following link: https://psl.noaa.gov/data/climateindices/list/. These indices represent high (ONI) and low (PDO and AMO) frequency modes of climate variability.

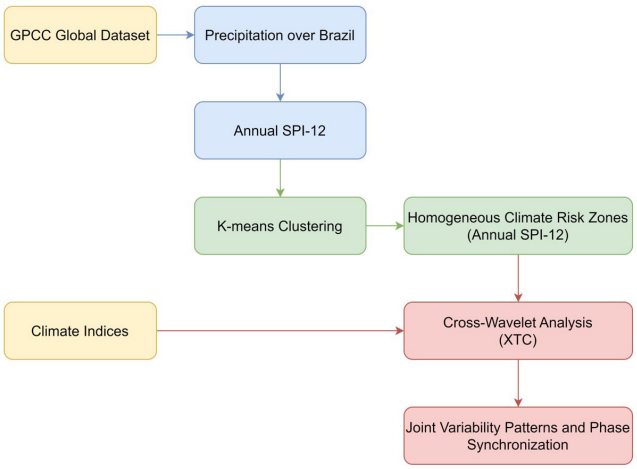

Figure 1. Graphical summary of the methodology employed. The yellow colors represent the input data; blues colors the processes of the standardization of the precipitation time series (Step 1); green colors the determination of the SPI time series clusters (Step 2) and red colors the XTC application.

Standard Precipitation Index

The Standard Precipitation Index (SPI) was first proposed by McKee et al. (1993), designed to be a versatile tool for analyzing meteorological droughts as it uses only precipitation data for its determination.

This index can be determined for a variety of time scales on which monthly precipitation is aggregated. This is a positive point, as it provides flexibility in assessing the effects of precipitation deficits on water resources at different scales, e.g., short time scales reflect impacts on soil moisture while long time scales reflect impacts on surface water availability (McKee et al. 1993).

The determination of the SPI consists of approximating the precipitation time series aggregated on an n-month scale to a Cumulative Distribution Function (CDF), making it possible to determine the probability of non-exceedance of the aggregated precipitation. From these probabilities the SPI can be calculated through the inverse function of the standard normal distribution, as presented in Equation 1 (Rocha et al., 2019; McKee et al., 1993).

$$SPI = \phi^{-1}\left[H(x)\right] \quad (1)$$

where: x is the aggregated precipitation at the adopted scale for SPI; $H(x)$ is the CDF that returns the probability of non-exceedance of event x; ϕ^{-1} is the inverse function of the standard normal distribution (ϕ), which has mean zero and unit standard deviation. By definition, the SPI represents the number of standard deviations that a specific value of aggregated precipitation in a n-month time scales has in relation to the average of a standardized normal distribution derived from the long-term time series of this variable.

In this study, we adopted a 12-month scale for the SPI (SPI-12), calculating it for each of the GPCC grid points in Brazil. To determine it, we adopted the CDF Gamma for all grid points. Based on the Komolgorov-Smirnov test, the gamma distribution fits around ~72% of the GPCC points considered. We consider this to be a satisfactory performance for this present article.

We chose to use the 12-month scale for the SPI because this time scale is more appropriate for analyzing drought events in environments with well-defined seasonality (Colombo et al., 2024; Ribeiro Neto et al., 2022). In these environments, time scales shorter than 12 months can interpret the reduction in rainfall during the dry season as a meteorological drought. In fact, this seasonal drought during the dry season is a meteorological drought, however, it is less relevant because low rainfall is already expected during this season. Therefore, and aiming to assess climate risk from an interannual perspective, the 12-month time scale was adopted for the SPI.

The above-mentioned procedures for SPI determination return a continuous monthly series of this index, which shows a dependency between its consecutive values. As mentioned by Estácio et al. (2021), the aggregated precipitation to determine the SPI-12 for two consecutive months differs in only 1 of the 12 aggregated values. Therefore, in order to remove this redundancy, we decided to use only the last month of each of the years that made up the monthly SPI-12 time series, resulting in an annual SPI-12 series that provides information on the accumulated rainfall between January and December of each year.

Although some Brazilian regions have rainfall cycles that begin in one year and end in the following year, we chose to standardize the climate risk analysis in the same current year, making it easier to get a picture of the associated risk at that time (year-end). This temporal standardization would facilitate planning and preparation for action at the national level.

In view of the transformation of the monthly SPI-12 series into an annual series, we also made adjustments to the monthly time series of the considered climate indices in order to make the XTC analyses feasible, transforming them into annual series by averaging all the months of each year.

Cluster analysis

The homogeneous climatic risk zones were determined using the K-means technique to determine homogeneous groupings of the annual SPI-12 series of the used GPCC grid points.

K-means is a clustering technique widely used in a variety of areas due to its simplicity, rapid implementation, ability to operate large databases, among other benefits (Ghasempour et al., 2022).

Roushangar et al. (2021) point out that k-means can be summarized in just two alternating steps: i) the assimilation step and ii) the update step. In the assimilation step, each observation is assigned to the cluster whose centroid has the smallest squared Euclidean distance from that point. In the update stage, the centroid is recalculated based on the assimilated points by each cluster and the aforementioned assimilation process is repeated. The loop between these two processes continues until no significant changes are observed in the update of the centroids

The number of clusters (n) in the K-means method needs to be defined before initializing the two alternating steps abovementioned. In this work, we defined n according to the Sum of Squared Euclidean Distances (SSED) of the samples to their respective centroids with which they are associated. The SSED was determined for values of $n \in [1,10]$, calculating its percentage variation between two consecutive values of n as shown in Equation 2:

$$\Delta SSED = \frac{\sqrt{\left(SSED(n) - SSED(n-1)\right)^2}}{SSED(n-1)} \quad (2)$$

where: ΔSSE is the percentage change in SSED between the numbers of clusters n and $n-1$; $SSE(n)$ and $SSE(n-1)$ are the SSED values for a number of clusters n e $n-1$, respectively.

This strategy for determining the number of clusters seeks to identify a point of convergence of the SSED, where two SSED values for two consecutive n do not show large percentage variations. Thus, from this point onwards, the increase in n to reduce the SSED is considered inefficient, making n the candidate for the number of clusters to be adopted.

It should be noted that SSED will always be decreasing as n tends to the sample size (k), because for $n = k$, $SSED = 0$, so each sample will be its own centroid. This strategy, therefore, does not aim to minimize SSED, but rather to find the point from which the increase in n will represent small variation in its value.

Finally, it is important to note that K-Means optimizes an objective function based on Euclidean distance, so it is very sensitive to the magnitude of the values. Therefore, it is common to standardize the database before applying this method. In this analysis, the standardization procedure was not necessary as the SPI is already a standardized index.

Cross-wavelet analysis (XTC)

Cross wavelet analysis (XTC) was used to map the common power variability patterns between the time series of the centroids of the delimited clusters and the considered climate indices: ONI, AMO and PDO. In addition, this analysis provided information on the synchronization between the phases of the periodic components of these two times series.

The Wavelet Transform (WT) enables analysis of the multi-frequency patterns that make up the original time series, and is a widely used for determining the dominant variability modes and the variation of these modes over a stationary or non-stationary time series. The original signal is decomposed in the time-frequency domain by translating and dilating a base generating function (mother wavelet) which produces a set of functions (daughter wavelets) of varying frequency, due to dilation, and varying positioning along the signal, due to translation. The translation and dilation procedures of the mother wavelet in the WT are expressed by the convolution integral shown in Equation 3:

$$W(t,s) = \frac{1}{\sqrt{s}} \int \psi_b \left(\frac{t'-t}{s} \right) X(t)\, dt \quad (3)$$

where: $W(t,s)$ is the generated wavelet coefficient; is the complex conjugate of ψ defined in time and scale; $\sqrt{s}$ corresponds to a

normalization factor for each wavelet's energy, seeking to maintain the same energy as the parent wavelet (Lima et al., 2021; Rocha & Souza Filho, 2020; Rocha et al., 2019; Torrence & Compo, 1998).

The generating function can be discrete or continuous. For each of these types of wavelets, there are a variety of base functions, each with its own specific characteristics and best suited to certain applications (Torrence & Compo, 1998). In this study, we used the Morlet wavelet as a generating function. This wavelet is a continuous function recommended by Torrence & Compo (1998) for the analysis of geophysical variables.

The mapping of common power regions in XTC is defined according to Equation 4:

$$W_n^{XY}(t,s) = \frac{1}{s} W_n^X(t,s) * W_n^Y(t,s) \quad (4)$$

where: W_n^{XY} is the Cross-Wavelet Transform; $W_n^X(t,s)$ and $W_n^Y(t,s)$ are the WT of the time series $X(t)$ and $Y(t)$. The power of the cross wavelet, in turn, is given by the modulus of W_n^{XY} (Rocha et al., 2019; Rocha & Souza Filho, 2020; Roesch & Schmidbauer, 2018).

In parallel to mapping the joint variability patterns across regions of common power, XTC makes it possible to assess the synchronization between the phases of the periodic components of $X(t)$ and $Y(t)$. Roesch & Schmidbauer (2018) presented a graphical interpretation of the relationship between the phases of these periodic components. In this interpretation, the different lag patterns are defined as a function of the argument W_n^{XY} (Figure 2).

RESULTS

Homogeneous climate risk zones

Figure 3 shows the percentage changes in SSED for the SPI-12 annual series used in the cluster analysis. It can be seen that the lowest levels of SSED percentage variation start at $n = 7$ (~3.5%), i.e., SSED for $n = 7$ decreased by around 3.5% compared to SSED for $n = 6$. The percentage change remains at a similar level until $= 10$ (~2.5%).

Based on the percentage variations in Figure 3, we adopted $n = 7$ as the main candidate for the number of clusters. We confirmed this value of n through some empirical tests, which consisted of analyzing the spatial continuity of the delimited regions by the clusters for n between 7 and 10 $(n \in [7,10])$. We found that for $n = 7$, the cluster analysis returned a good spatial continuity of the delimited regions with the lowest number of clusters among the tested values. Therefore, $n = 7$ was adopted for the cluster analysis of the SPI-12 series using the K-Means technique.

Figure 4 shows the clusters of GPCC grid points over Brazilian territory for the annual SPI12 time series and the centroid time series of these clusters. The time series of the members that make up each of these clusters have been plotted in light gray against the background of the time series of the cluster centroids.

It should be noted that the regions delimited by the 7 clusters showed good spatial continuity. Clusters 1 and 5 were entirely contained in the northern region of Brazil, covering most of that region. Cluster 2 was mostly located in the north of Brazil's northeastern region, extending to the eastern portion of the northern region. Cluster 3 covered the southern region of Brazil, extending slightly into the southern portions of the Southeast and Midwest. Cluster 4 encompassed the southern portion of the Northeast region of Brazil and small portions of the Southeast of the North region and of the West of the Central-West region. Cluster 6 was located in the central part of the Southeast region of Brazil, with a small part located in the Southeast of the Centra-West region of Brazil. Finally, cluster 7 was situated in the Central-West region of Brazil, with small parts in the South-West of the South-East region and the South of the North region.

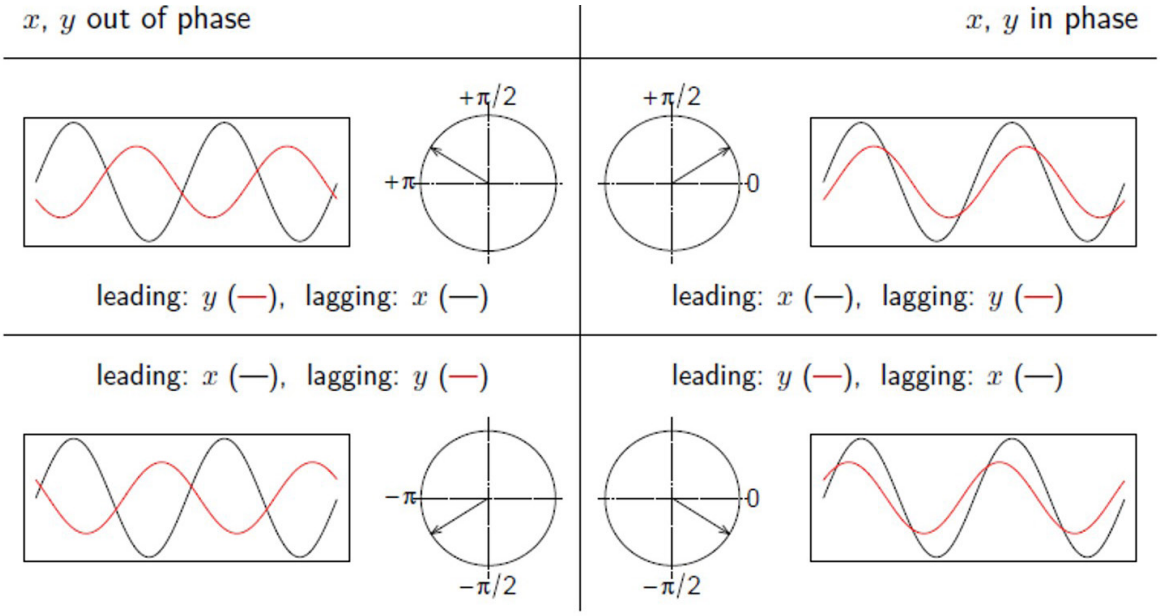

Figure 2. Lag patterns of two periodic components in the XTC. Source: Roesch & Schmidbauer (2018).

The centroid time series of the defined clusters (Figure 4) exhibit signs of interannual variability. It is worth noting the strong attenuation of the variability of the clusters' centroid time series in relation to the time series of the members that make up these clusters, especially for Cluster 1.

Despite the similarity between some regions, there was a heterogeneity in the variability of the centroid time series between some clusters, varying the amplitude and direction of the variation. Clusters 1 and 5, for example, showed divergences in the SPI12 signals (positive or negative) in some years, and cluster 5 showed a greater amplitude of variation between years. Clusters 2 and 3, located in the northeast and south of Brazil, respectively, showed divergent behavior, with the positive (negative) peaks of cluster 2 occurring negative (positive) peaks of the cluster 3.

Clusters 2 and 4, although mostly located in the Northeast, show some significant divergences between their centroid time series. Despite some simultaneous occurrences of positive and negative extremes of the SPI12 in these two clusters, there is more pronounced inter-annual variability in cluster 4, even reaching more extreme negative values than cluster 2.

The centroid of cluster 6 showed the greatest amplitude of variation, with minimum SPI12 values below −3 and maximum values above +2. The occurrence of extremes in its time series is similar to the occurrence of extremes in clusters 2, 3 and 4. This similarity is, in some cases, for extremes in the same direction, for example: negative extremes in 1990 in clusters 2, 4 and 6; positive extremes in 1983 in clusters 3 and 6; positive extremes in 1992 in clusters 4 and 6. In other cases, opposite extremes are observed in cluster 6 in relation to these aforementioned clusters: positive peak in cluster 6 and negative peak in cluster 2 in 1983; positive peak in cluster 6 in 1992 and a sequence of negative values between 1990 and 1993 in cluster 2; negative peak in 2014 in cluster 6 and positive peaks in cluster 3 present in 2014 and 2015.

Cluster 7's centroid time series was, along with cluster 1's, the one with the smallest amplitude of variation. The temporal evolution of its centroid is quite distinct, however, some short periods are similar to those of the other clusters, for example, between 1972 and 1980 the behavior of its centroid is similar to that of cluster 1, with exclusively positive SPI12 values. It is remarkable that, from 1980 onwards, there was a predominance of negative SPI12 values in Cluster 7, forming a downward trend with minimum values occurring between 2010 and 2020.

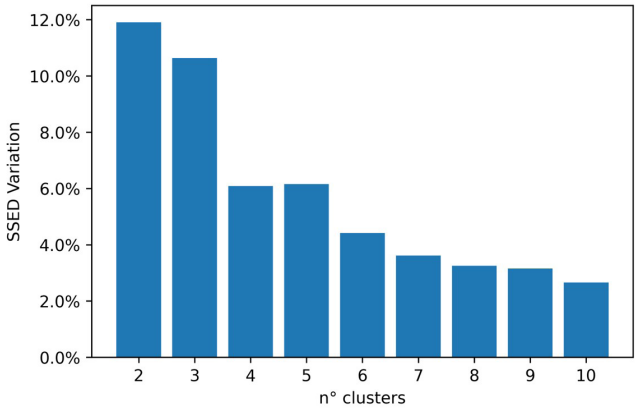

Figure 3. Percentage variation of the Sum of Squared Euclidean Distances (SSED) for the SPI-12 annual series for number of clusters between 2 and 10.

Cross-wavelet analysis

Due to the large number of XTC analyses carried out (7 clusters and 3 climate indices, resulting in a total of 21 XTC analyses), we decided to only evaluate the regions that showed statistical significance for the joint periodicity hypothesis (alternative hypothesis), i.e. regions that showed a significance level of less than 0.05. Furthermore, we opted to present a detailed description of the mapped joint variability patterns in Supplementary Material A, keeping a summary description of these results in this article.

Clusters' centroid and ONI climate index

Figure 5 presents the cross-wavelet power spectrums of the clusters' centroid time series presented in Figure 4 and the ONI climate index. The arrows indicate the relationship between the phases of the periodic components of this index (y) and the Cluster centroid time series (x).

The statistically significant regions with the greatest power were contained in the 2 to 8 year band for all the clusters. Cluster 1 exhibited areas of statistical significance in the 2 to 4 year, 4 to 8 year and 8 to 16 year bands, with an out-of-phase and leading pattern in all of them.

Clusters 2, 3 and 5 showed statistically significant areas in the 3 to 6 year, 6 to 8 year and 8 to 16 year bands. Despite the similarity of the bands, these clusters showed distinct joint variability patterns. Clusters 2 and 5 alternated between a leading and lagging out-of-phase patterns. Cluster 3, on the other hand, showed in-phase patterns that alternated between slightly leading and slightly lagging for the different bands and for the same band in different period.

Cluster 4 presented a single area with statistical significance in the 3 to 6 year band with an out-of-phase and lagging pattern. Cluster 6 showed statistically significant regions in the 2 to 4 year, 3 to 6 year and 12 to 16 year bands, with an out-of-phase and leading pattern in the first band; in-phase and slightly leading pattern in the second band and alternating between these two patterns at different times in the last band. Cluster 7, despite regions with high power in the 2 to 4 year band throughout the series, only showed statistically significant regions in the ~4 year and 15 to 24 year bands with out-of-phase and leading pattern.

Clusters' centroid and PDO climate index

Figure 6 presents the cross-wavelet power spectrums of the clusters' centroid time series presented in Figure 4 and the PDO climate index. The arrows indicate the relationship between the phases of the periodic components of this index (y) and the Cluster centroid time series (x).

XTC analysis between the determined cluster centroids and the PDO climate index delineated areas with statistical significance

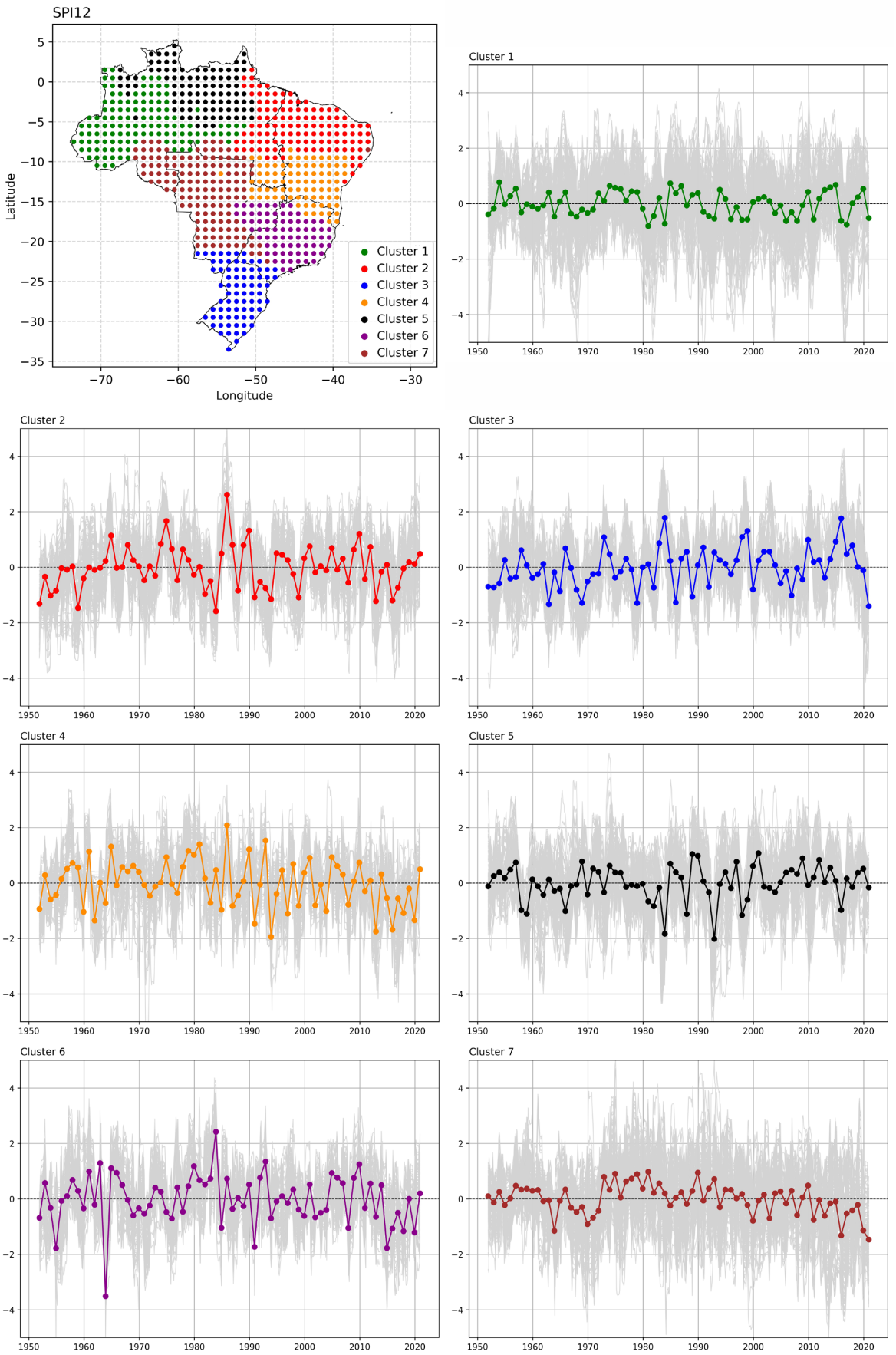

Figure 4. Brazilian Homogeneous Climate Risk Zones and time series of the centroids of the clusters for $n=7$. In the time series of the centroids, all members that make up the cluster are plotted behind in light gray.

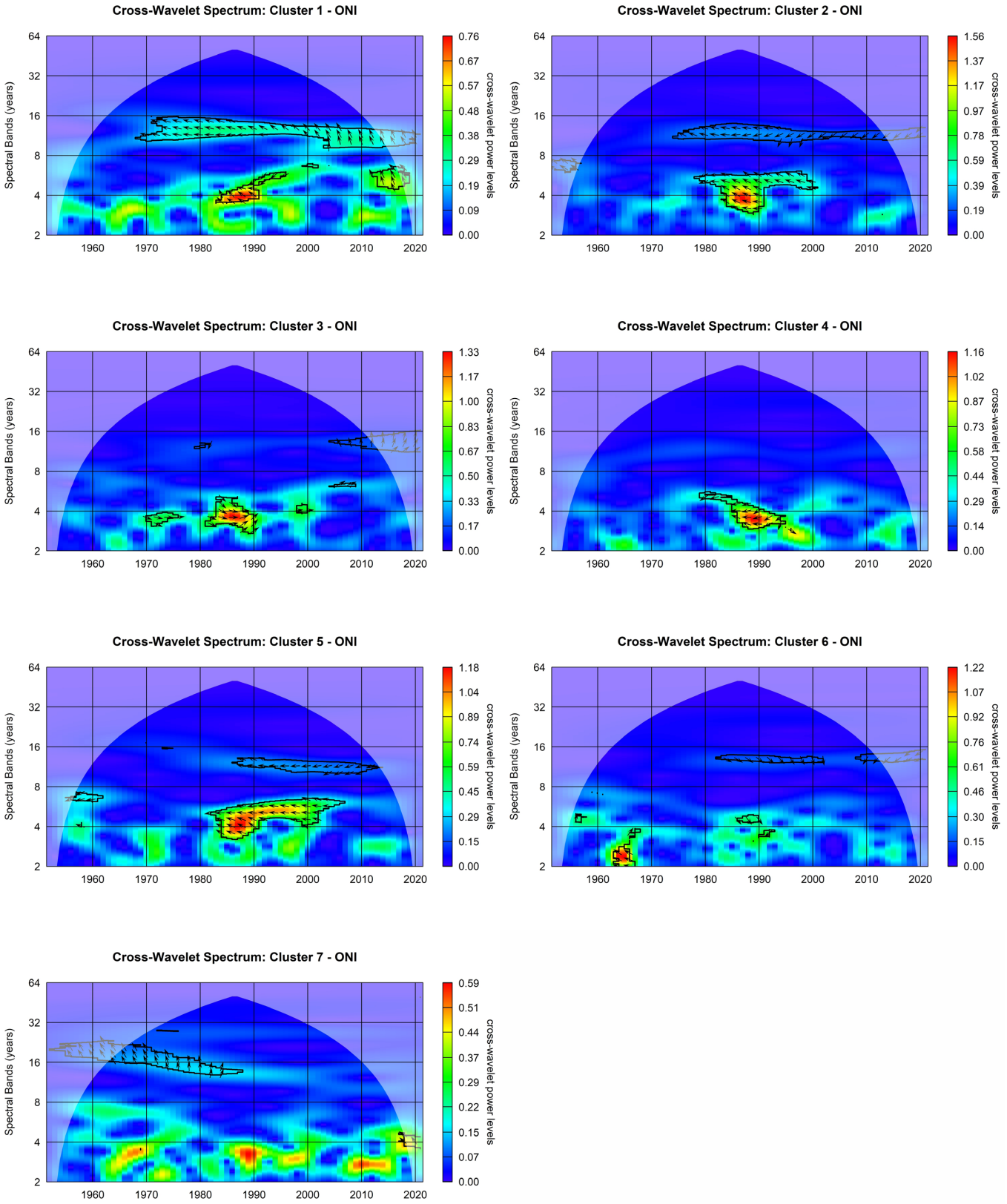

Figure 5. XTC between the clusters' centroid time series and the ONI climate index.

in the 8 to 16 year and 32 to 64 year bands in all cases. For some clusters, small areas with statistical significance were also formed in the 2 to 4 year and 4 to 8 year bands.

Cluster 1 showed statistically significant areas in the 4 to 8 year bands that alternated between leading and lagging out-of-phase patterns throughout the time series; in the 8 to 16 year band

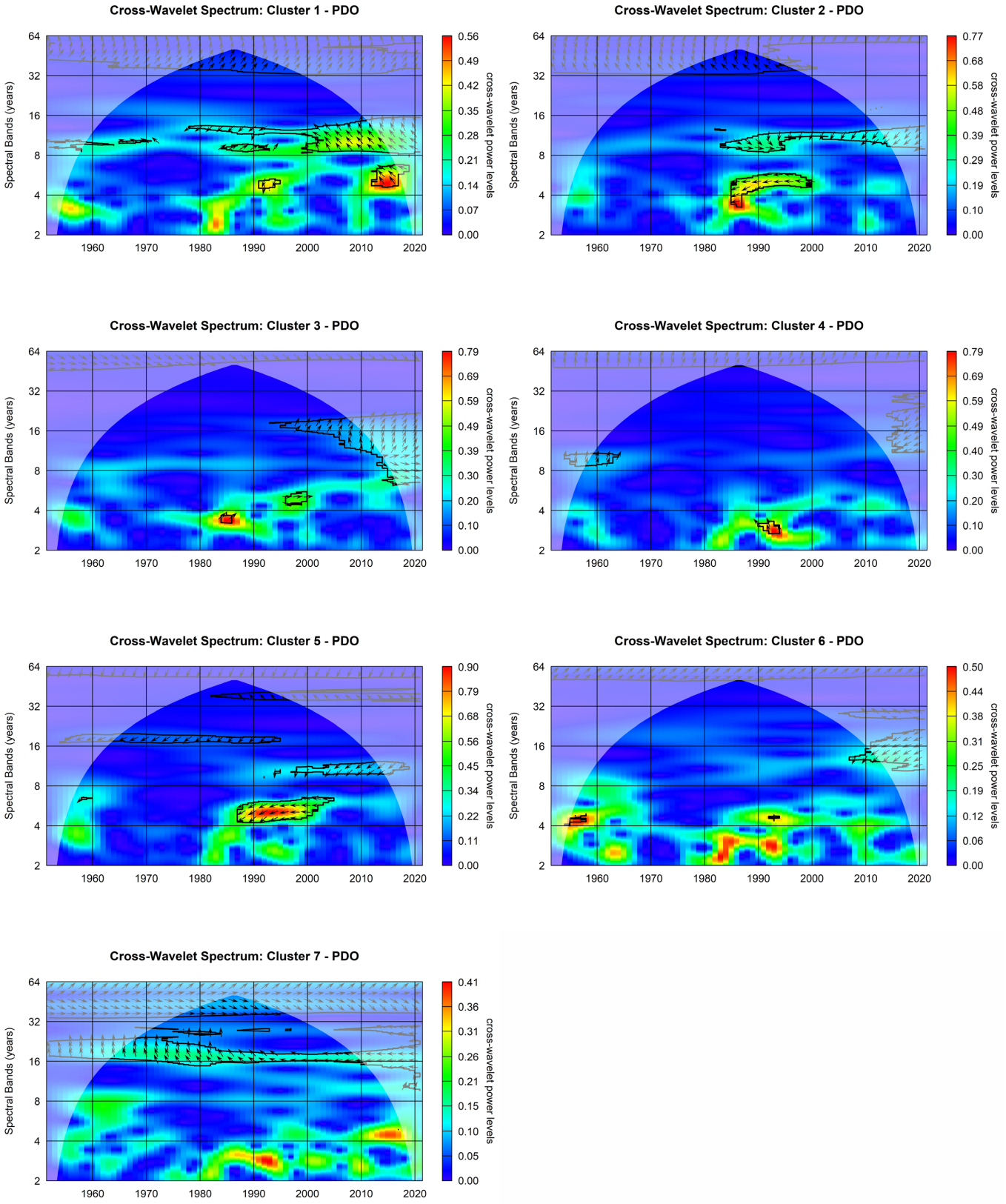

Figure 6. XTC between the clusters' centroid time series and the PDO climate index.

with out-of-phase and leading patterns with some occurrences of out-of-phase and slightly lagging patterns and in the 32 to 64 year band with a out-of-phase and slightly lagging pattern.

The regions with statistical significance for Cluster 2 were contained in the bands from 3 to 6 years with an out-of-phase and lagging pattern; in the band from 8 to 16 years alternating between

in-phase and slightly leading and out-of-phase and lagging patterns and in the band from 32 to 64 years mostly with an in-phase and slightly lagging pattern. Cluster 3 presented statistically significant areas in the 2 to 4 year, 4 to 8 year, 8 to 16 year and 48 to 64 year bands, the first three with an in-phase and slightly lagging pattern and the last with an in-phase and slightly leading.

Cluster 4 showed statistically significant areas in the 2 to 4 year, 8 to 16 year, 16 to 32 year and 32 to 64 year bands with out-of-phase and leading, in-phase and slightly lagging, out-of-phase and lagging and in-phase and slightly lagging patterns, respectively. For Cluster 5, the regions with statistical significance were contained in the 4 to 8 year, 8 to 16 year, 16 to 32 year and 32 to 64 year bands with out-of-phase and lagging patterns, except for a region between the ~32 and ~48 year periods which showed an out-of-phase and leading pattern.

Cluster 6 showed few areas of statistical significance, but those delimited were located in the 12 to ~20 year, 24 to 32 year and 48 to 64 year bands with out-of-phase and lagging, out-of-phase and leading and in-phase slightly lagging patterns, respectively. Finally, Cluster 7 showed statistical significance in the 16 to 24 year bands, with an out-of-phase and leading pattern, and in the 32 to 64 year band, alternating between slightly leading (32 to ~48 years) and slightly lagging (~48 to 64 years) in-phase patterns.

Clusters' centroid and AMO climate index

Figure 7 presents the cross-wavelet power spectrums of the clusters' centroid time series presented in Figure 4 and the AMO climate index. The arrows indicate the relationship between the phases of the periodic components of this index (y) and the Cluster centroid time series (x).

The areas with statistical significance in the XTC between the delimited clusters and the AMO index were contained in frequency bands with higher periods. In clusters 1 and 2 they were contained in the 8 to 16 year bands (out-of-phase and leading pattern) and in the 32 to 64 year band (out-of-phase and lagging pattern), the latter cluster also showed a small region in the 2 to 4 year band with an out-of-phase and lagging pattern.

The statistically significant regions of Cluster 3 were situated in the 8 to 16 year, ~16 year and 48 to 64 year bands, with out-of-phase and lagging, in-phase and slightly lagging and alternating between positive phase and in-phase and slightly leading patterns, respectively. Clusters 4, 5 and 6 showed statistically significant regions in the 32 to 64 year band with out-of-phase and lagging, in-phase and slightly leading and out-of-phase and leading patterns, respectively.

Cluster 7 exhibited an extensive region with statistical significance in the 16 to 64 year band, which showed two distinct patterns throughout: in-phase and slightly lagging between 16 and 32 years and out-of-phase and leading between 32 and 64 years.

DISCUSSIONS

Homogeneous climate risk zones in Brazil

The homogenous climate risk zones delineated with the annual SPI12 series showed good spatial continuity. These areas can be related to the influence areas of meteorological systems that operate in Brazil.

The arrangement of Clusters 1 and 5 in the northeast/north and southwest/south portions of the northern region of Brazil, respectively, reveals the spatial variability of precipitation patterns within the same Brazilian biome (Amazon). The spatiotemporal variation in precipitation over the Amazon region is explained by the action of large-scale and synoptic-scale convective systems, such as: i) the ITCZ and the Coastal Squall Line (CSL), acting mainly in the north and northeast, ii) the SACZ and the Bolivian High, acting mainly in the south and southwest of the Amazon (Lucas et al., 2021; Marengo & Espinoza, 2016).

Cluster 2, located in the northern part of the Northeast region, encompasses a region where annual precipitation volumes are directly related to the latitudinal position of the ITCZ (Marengo et al., 2017, 2018, 2022; Reboita et al., 2010) and the influence of easterly waves disturbances on its coastal portion (Reboita et al., 2010).

Given the disposition of Clusters 2 and 5 in Brazilian territory, it can be stated that the ITCZ has a major influence on precipitation volumes in a region that extends from the north of the Northeast region to the north of the Northern region. However, this region was encompassed by two distinct clusters, which can be explained by the convective processes characteristic of tropical forests. As reported by Staal et al. (2018), the Amazon forest recycles around 32% of its evapotranspiration, i.e. 32% of evapotranspiration losses return to the Amazon region in the form of precipitation. This characteristic, among others, is one of the main distinctions that can be made between the regions in Clusters 2 and 5.

The Cluster 3, located in southern Brazil, encompasses a region in which annual precipitation volumes depend on the formation of Cold Fronts (Lima et al., 2021; Grimm et al., 2020). One of the characteristics of this region is the good distribution of precipitation volumes throughout the year, with high annual precipitation volumes (Reboita et al., 2010). Reboita et al. (2010) also highlight the indirect influence of the SACZ on annual precipitation volumes.

Clusters 1, 4, 6 and 7, located in the south-central regions of Amazonia, the Midwest, the Southeast and the south-central region of Bahia, respectively, have their precipitation regime directly influenced by the SACZ. The SACZ is a band of cloudiness and precipitation that acts in a northwest-southeast direction over Brazil, occurring during the warm season in South America (Nov-Mar). This system transports moisture from tropical to subtropical latitudes when it is active, playing a major role in the rainfall regime over its action area (Pezzi et al., 2023; Fialho et al., 2023).

Despite the predominant role of the SACZ in the precipitation regime within its action area, different clusters can be observed throughout it. This discontinuity (different clusters) can be explained by a number of factors, such as the joint influence of different meteorological systems acting on different space-time scales, the type and characteristics of the biome or even different levels of SACZ influence due its complex spatial characteristics. Regarding its spatial characteristics, Fialho et al. (2023) point out that the SACZ can be classified into two types: Oceanic and Continental, and can occur independently or in a connected way. Carvalho et al. (2011) emphasize that these two types should be seen as distinct

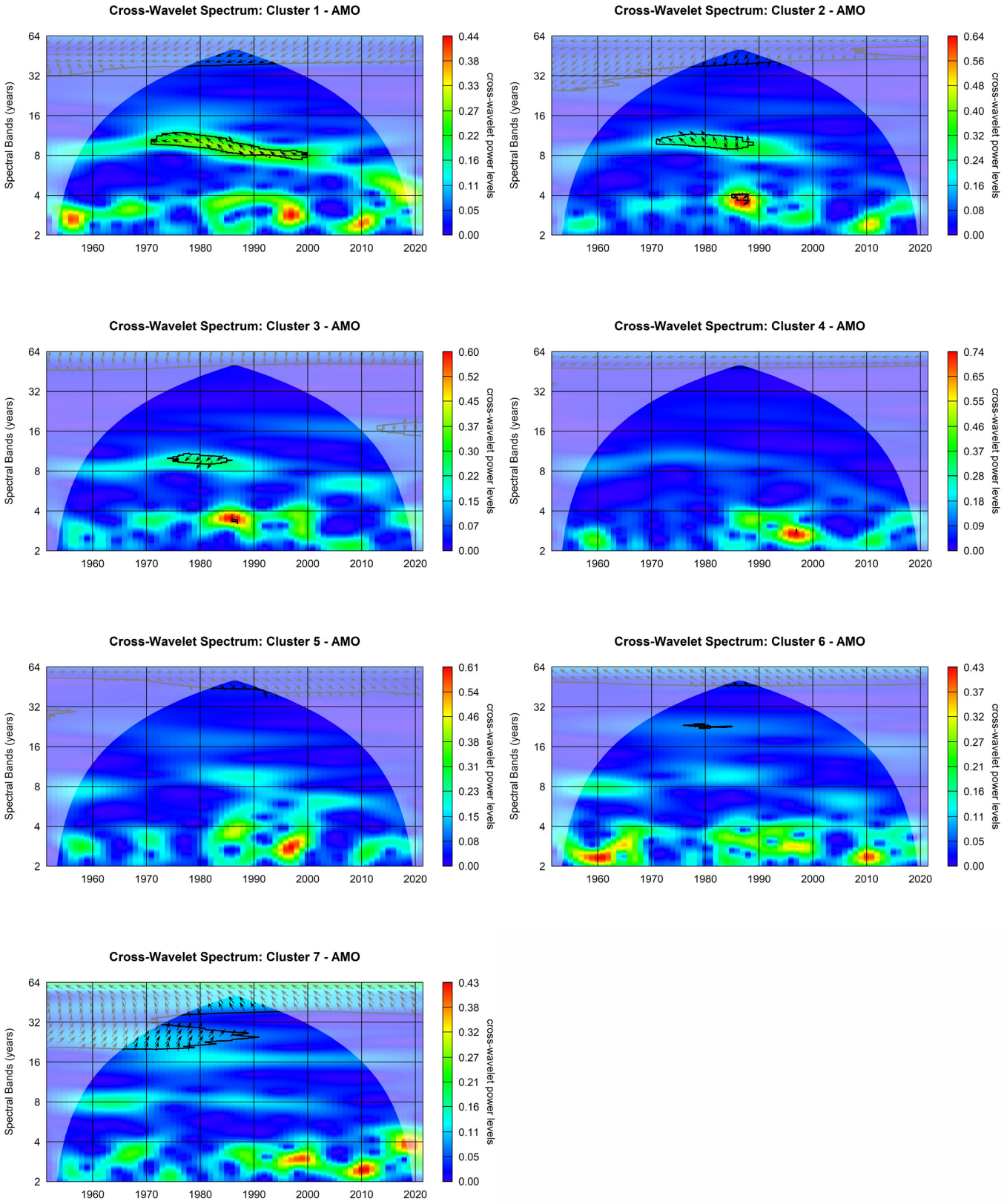

Figure 7. XTC between the clusters' centroid time series and the AMO climate index.

variability modes in convective activity, e.g., in coastal regions there will be a greater influence of oceanic SACZ activity, regardless of the rainfall regime in the continental portion of the SACZ.

It is worth noting that the regions of homogeneous climatic risk in Brazil (Figure 4a) are similar to the division of climatological precipitation in Brazil. Based on the annual rainfall

cycles in South America presented by Grimm (2011), it can be seen, for example, that the northeastern and northern regions of Brazil have different climatological precipitation in their northern and southern portions, similar to the division made by Cluster 2 and Cluster 4 and by Cluster 1 and Cluster 5, respectively. In addition, the southern region of Brazil has a different annual rainfall cycle than the other regions, a distinction similar to that of Cluster 3 (Figure 4a). These similarities are to be expected because, as mentioned above, the homogeneous climate risk zones can be related to the influence areas of meteorological systems that act in Brazil, which modulate and define the main characteristics of the annual precipitation cycles in Brazilian territory.

Despite these similarities, the annual rainfall cycles presented by Grimm (2011) point to similar climatological precipitation between the Central-West and Southeast regions, except for the coast of the latter. The delineated homogeneous climate risk regions delimited, in turn, indicate two distinct groupings for these regions: Cluster 6 and Cluster 7, respectively.

Influence of climate variation modes

The XTC analysis pointed to different joint variability patterns between the time series of the cluster centroids and of the analyzed climate indices, varying both the periodicity of this variability and the direction of their relationship (out-of-phase or in-phase) between the different centroids as well as over the analyzed period (1951 to 2020) for the same centroid.

The ONI climate index showed an out-of-phase joint variability pattern for clusters 1, 2, 4, 5 and 7, alternating between lagging and leading, and an in-phase pattern for cluster 3, alternating between slightly lagging and slightly leading. Cluster 6, on the other hand, exhibited periods with an in-phase variability pattern and other periods with an out-of-phase pattern. Except for the Cluster 7, the regions with statistical significance were contained in the 2 to 8 year and 8 to 16 year bands, with a high power of crossed wavelets in the first case.

The out-of-phase patterns suggests that the positive (negative) phases of the ONI negatively (positively) influence precipitation volumes in the regions encompassed by the abovementioned clusters. The high cross-wavelet powers in the statistically significant regions of the 2 to 8 year band indicate a strong influence on the interannual variability of precipitation.

In relation to the clusters on the ITCZ's influence on their precipitation volumes (Clusters 2 and 5), several authors point to the influence of the warming (cooling) of the equatorial Pacific in reducing (favoring) precipitation volumes during the rainy season in these regions (Pontes Filho et al., 2020; Cunha et al., 2019; Marengo et al., 2017, 2018; Marengo & Espinoza, 2016; Grimm, 2011).

Marengo et al. (2017) highlight that the influence of the El Niño Southern Oscillation (ENOS) on the interannual variability of the Brazilian Northeast is mainly due to changes in the Walker cell resulting from the warming of the equatorial Pacific. This change establishes the descending branch of this cell over the North/Northeast region of Brazil, forming a high-pressure region that hinders convective processes. Moreover, it can culminate in an anomalous more northerly positioning of the ITCZ during the peak precipitation months (Feb-Apr), when associated with a positive inter-hemispheric gradient of the SST in the Atlantic Ocean, negatively impacting the precipitation volumes of the region's rainy season (Cai et al., 2020).

In the Northern region, Marengo & Espinoza (2016) underline the importance of the temperature anomalies of the equatorial Pacific in the interannual variability of precipitation, presenting a history of droughts and floods related to El Niño and La Niña episodes, respectively, demonstrating the out-of-phase joint variability pattern between annual precipitation and the ONI climate index that monitors this phenomenon.

The Walker cell change due to the warming of the equatorial Pacific may also explain the in-phase joint variability pattern between Cluster 3 and the ONI index. The establishment of a high-pressure zone as a result of the downward movements of the upper atmosphere over the North and Northeast of Brazil prevents the natural movement of cold fronts (south to north), increasing their permanence over the southern region and, consequently, favoring precipitation volumes.

The aforementioned modulation patterns of annual precipitation in the North/Northeast and South of Brazil are corroborated by Grimm (2011). Grimm (2011) points out that ENSO is the main mechanism of interannual variability in South America, with positive (negative) anomalies being observed in southern Brazil and negative (positive) anomalies in the northeastern part of South America during El Niño (La Niña) events.

Regarding the SACZ-influenced regions (Clusters 1, 4, 6 and 7), the ENSO phases also modulate the occurrence of this atmospheric system, affecting the annual precipitation regime in these regions. Carvalho et al. (2004) report that the ENSO phases influence the frequency of SACZ events, modulating their two types of occurrences differently, with the warm (cold) phase favoring the occurrence of oceanic (continental) SACZ.

The distinct influence of the ENSO phases on the oceanic and continental SACZ may explain the out-of-phase joint variability patterns in Clusters 1, 4 and 7 and the in-phase periods in Cluster 6. It is worth noting that the regions with statistical significance and in-phase join variability pattern in Cluster 6 occurred between 1980 and 2000, a period characterized by a warm phase of the PDO (Rocha & Souza Filho, 2020) and recurring years with strong El Niño 1982-83, 1986-87, 1991-92, 1997-98 (Climate Prediction Center, 2024).

The XTC for the PDO and the clusters' centroid time series identified statistically significant zones in the 4 to 8 year, 8 to 16 year, 16 to 32 year and 32 to 64 year bands, suggesting climate modulation on decadal and multidecadal scales in addition to the interannual one. Kayano et al. (2019) point out that the PDO modulates interannual climate variability in different regions of the planet. Rocha & Souza Filho (2020) indicate that the duration of the PDO phase varies between 13 to 22 years.

It is interesting to note that the joint variability patterns were similar to those observed for the ONI index. Clusters 2 and 5, for example, showed a mostly out-of-phase pattern, suggesting that the positive (negative) phases of the PDO negatively (positively) influence rainfall in the cluster regions. Cluster 3, on the other hand, showed an in-phase pattern, with positive phases favoring precipitation in the cluster region and vice versa.

This similar behavior can be explained by the modulation of high-frequency modes of variability, e.g. ONI, by low-frequency

ones. With regard to ENSO, its influence on rainfall variability over South America, and more specifically over Brazil, is intensified when its phase coincides with the PDO phase, i.e. El Nino and Warm PDO (WPDO) and La Niña and Cold PDO (CPDO) (Kayano et al., 2019, 2020).

The XTC for the AMO index and the Clusters centroid time series showed statistically significant zones in the 8 to 16 year bands (Clusters 1, 2 and 3) and in the 32 to 64 year band (in all Clusters), suggesting modulations on decadal and multidecadal scales. As presented by Kayano & Capistrano (2014), the anomalous Walker cell that connects the Tropical Pacific to the Equatorial Atlantic leads to a strengthening of El Niño (La Niña) during the cold (warm) phase of the AMO.

Study limitations and futher analysis

Although the presented results satisfy the objective of this work: "delineate the homogeneous climate risk zones throughout Brazilian territory", we understand that climate risk consists of a complex network of feedbacks between various physical processes and human-nature relations, which have not been fully taken into account in the presented analyses. For future studies, we believe it is essential to deepen our understanding of the vulnerabilities imposed by Brazil's socioeconomic inequalities and expand the list of climate variability mechanisms, including analyzing processes/phenomena that occur on a smaller scale than the interannual one and the possible iterations between them.

Another pertinent point is the use of a single statistical distribution for all the GPCC grid points. Although the Gamma distribution fits ~72% of all GPCC grid points, it is possible that the SPI values at the other points do not adequately represent the precipitation anomalies, especially in years with climatic extremes. This misrepresentation of precipitation anomalies can affect the process of clustering the SPI series, leading to errors in the delineation of homogeneous climate risk zones. For future studies, we recommend evaluating a set of statistical distributions for each grid point and selecting the one with the best performance in determining the SPI.

Regarding the XTC analysis between the cluster centroids and the considered climate indices, the variations of the joint variability patterns over time indicate the non-stationarity of the cluster centroid time series. Although not discussed in detail in this paper, these variations are worth highlighting and undoubtedly provide valuable information for proactive climate risk management across the homogeneous climate risk regions identified in Brazil. In this context, we recommend that future studies address this matter in more detail.

Finally, we recommend that future studies assess whether the use of other precipitation databases, such as Xavier et al. (2022) or CHIRPS (Funk et al., 2015), can improve the obtained results.

CONCLUSIONS

In this study, the K-means technique was used to define Brazil's homogeneous climate risk zones considering the annual SPI-12 time series of all the GPCC grid points contained in Brazilian territory, assessing their possible associations with large-scale SST oscillations represented by the ONI, PDO and AMO indices.

The results showed significant climatic heterogeneity across Brazil, with different patterns of interannual variability, varying in amplitude and direction over the years. Regarding associations with large-scale oscillations in the SST, different patterns of modulation were found throughout Brazilian territory, which act on different time scales.

The seven defined clusters allowed for a satisfactory representation of Brazil's homogeneous climate risk zones, ensuring good differentiation and maintaining good spatial continuity of the delimited regions. From the results obtained and the discussions carried out, the main conclusions about the delimited regions can be summarized:

- Region 1 (Cluster 1) – Located in the west/south of the northern region of Brazil, it is influenced by the SACZ and the Bolivian High. It exhibits an out-of-phase relationship with the ONI, PDO and AMO climate indices, influencing its interannual (ONI) and decadal/multidecadal (PDO/AMO) variability;
- Region 2 (Cluster 2) – Located in the north of the Brazilian northeast, with a small extension in the eastern part of the northern region. This region is directly influenced by the ITCZ and, in its coastal part, of the Easterly Waves Disturbances. There is an out-of-phase relationship with the ONI, PDO and AMO climate indices, influencing its interannual (ONI) and decadal/multidecadal (PDO/AMO) variability;
- Region 3 (Cluster 3) – Situated in the South of Brazil, with a small extension to the South of the Southeast and Midwest regions. Annual precipitation volumes depend on cold fronts and an indirect influence from the SACZ. It has in-phase relationship with the ONI, PDO and AMO climate indices, influencing on its interannual (ONI) and decadal/multidecadal (PDO/AMO) variability;
- Region 4 (Cluster 4) – Situated in the southern portion of Brazil's northeast region, with small extensions in the north, southeast and central-west regions. This region corresponds to a portion of the continental SACZ's activity area. It shows an out-of-phase relationship with the ONI, PDO and AMO climate indices, influencing its interannual (ONI) and decadal/multidecadal (PDO/AMO) variability;
- Region 5 (Cluster 5) – Located in the north-central part of the northern region. This region is influenced by the ITCZ and the CSL. It presents an out-of-phase relationship with the ONI and PDO climate indices and an in-phase relationship with the AMO, influencing its interannual (ONI) and decadal/multidecadal (PDO/AMO) variability;
- Region 6 (Cluster 6) – Located in the central part of the Southeast, extending from its coastline to a small portion of the Southeast of the Central-West region. The Oceanic SACZ acts in this region, and the influence of High-Level Cyclonic Vortices (HLCVs) also stands out. It has periods/bands alternating between an in-phase and out-of-phase relationship with the ONI and PDO climate indices and out-of-phase with the AMO, influencing its interannual (ONI) and decadal/multidecadal (PDO/AMO) variability;

- Region 7 (Cluster 7) – Situated in the Brazilian Midwest with small extensions in the south of the northern region. This region corresponds to a portion of the continental SACZ's activity area. It shows an out-of-phase relationship with the ONI climate indices and periods/bands alternating between in-phase and out-of-phase with the PDO and AMO climate indices, indicating an influence on interannual, decadal and multidecadal variability (ONI, PDO and AMO).

The homogeneous climate risk zones delineated in this paper suggest the spatial limits for which a single climate risk management strategy can adequately and efficiently address this risk and promote better synergy and cohesion of adaptation measures. For example, a climate risk management strategy designed for Cluster 2 region may be inefficient for Cluster 3 region because it does not take into account all the climate risk features that exist in the latter region due to the climatic heterogeneity between them.

ACKNOWLEDGEMENTS

The present study was supported by the Fundação Cearense de Apoio ao Desenvolvimento Científica e Tecnológico (FUNCAP) and the Conselho Nacional de Desenvolvimento Científico e Tecnológico - Brasil (CNPq).

DATA AVAILABILITY STATEMENT

The data that support the findings of this study are openly available from the GPCC Full Data Monthly Product Version 2022 at http://dx.doi.org/10.5676/DWD_GPCC/FD_M_V2022_100 and from the Cold & Warm Episodes by Season at https://origin.cpc.ncep.noaa.gov/products/analysis_monitoring/ensostuff/ONI_v5.php.

REFERENCES

Aliaga, V. S., & Piccolo, M. C. (2021). Variability of extreme precipitation events in the Northeastern Argentine region. *Theoretical and Applied Climatology*, *145*(3-4), 955-965. http://dx.doi.org/10.1007/s00704-021-03659-0.

Cai, W., McPhaden, M. J., Grimm, A. M., Rodrigues, R. R., Taschetto, A. S., Garreaud, R. D., Dewitte, B., Poveda, G., Ham, Y.-G., Santoso, A., Ng, B., Anderson, W., Wang, G., Geng, T., Jo, H.-S., Marengo, J. A., Alves, L. M., Osman, M., Li, S., Wu, L., Karamperidou, C., Takahashi, K., & Vera, C. (2020). Climate impacts of the el niño–southern oscillation on South America. *Nature Reviews Earth & Environment*, *1*(4), 215-231. http://dx.doi.org/10.1038/s43017-020-0040-3.

Carvalho, L. M. V., Jones, C., & Liebmann, B. (2004). The south Atlantic convergence zone: intensity, form, persistence, and relationships with intraseasonal to interannual activity and extreme rainfall. *Journal of Climate*, *17*(1), 88-108. http://dx.doi.org/10.1175/1520-0442(2004)017<0088:tsaczi>2.0.co;2.

Carvalho, L. M. V., Silva, A. E., Jones, C., Liebmann, B., Dias, P. L. D., & Rocha, H. R. (2011). Moisture transport and intraseasonal variability in the South America monsoon system. *Climate Dynamics*, *36*(9-10), 1865-1880. http://dx.doi.org/10.1007/s00382-010-0806-2.

Coelho, C. A. S., Oliveira, C. P., Ambrizzi, T., Reboita, M. S., Carpenedo, C. B., Campos, J. L. P. S., Tomaziello, A. C. N., Pampuch, L. A., Custódio, M. de S., Dutra, L. M. M., Rocha, R. P., & Rehbein, A. (2016). The 2014 southeast Brazil austral summer drought: regional scale mechanisms and teleconnections. *Climate Dynamics*, *46*(11-12), 3737-3752. http://dx.doi.org/10.1007/s00382-015-2800-1.

Colombo, P., Ribeiro Neto, G. G., Costa, A. C., Mamede, G. L., & Van Oel, P. R. (2024). Modeling the influence of small reservoirs on hydrological drought propagation in space and time. *Journal of Hydrology*, *629*, 130640. http://dx.doi.org/10.1016/j.jhydrol.2024.130640.

Climate Prediction Center – CPC. (2024). *Historical El Niño/La Niña episodes (1950-present)*. Retrieved in 2024, May 05, from https://origin.cpc.ncep.noaa.gov/products/analysis_monitoring/ensostuff/ONI_v5.php

Cunha, A. P. M. A., Zeri, M., Deusdará Leal, K., Costa, L., Cuartas, L. A., Marengo, J. A., Tomasella, J., Vieira, R. M., Barbosa, A. A., Cunningham, C., Cal Garcia, J. V., Broedel, E., Alvalá, R., & Ribeiro-Neto, G. (2019). Extreme drought events over Brazil from 2011 to 2019. *Atmosphere*, *10*(11), 642. http://dx.doi.org/10.3390/atmos10110642.

Dhungana, S., Shrestha, S., Van, T. P., Kc, S., Das Gupta, A., & Nguyen, T. P. L. (2023). Evaluation of gridded precipitation products in the selected sub-basins of Lower Mekong River Basin. *Theoretical and Applied Climatology*, *151*(1-2), 293-310. http://dx.doi.org/10.1007/s00704-022-04268-1.

Estácio, Á. B. S., Silva, S. M. O., & Souza Filho, F. A. (2021). Statistical uncertainty in drought forecasting using Markov chains and the standard precipitation index (spi). *Revista Brasileira de Climatologia*, *28*, 471-493. http://dx.doi.org/10.5380/rbclima.v28i0.77590.

Fialho, W. M. B., Carvalho, L. M. V., Gan, M. A., & Veiga, S. F. (2023). Mechanisms controlling persistent South Atlantic Convergence Zone events on intraseasonal timescales. *Theoretical and Applied Climatology*, *152*(1-2), 75-96. http://dx.doi.org/10.1007/s00704-023-04375-7.

Funk, C., Peterson, P., Landsfeld, M., Pedreros, D., Verdin, J., Shukla, S., Husak, G., Rowland, J., Harrison, L., Hoell, A., & Michaelsen, J. (2015). The climate hazards infrared precipitation with stations--a new environmental record for monitoring extremes. *Scientific Data*, *2*(1), 150066. http://dx.doi.org/10.1038/sdata.2015.66.

Ghasempour, R., Roushangar, K., Ozgur Kirca, V. S., & Demirel, M. C. (2022). Analysis of spatiotemporal variations of drought and its correlations with remote sensing-based indices via wavelet analysis and clustering methods. *Hydrology Research*, *53*(1), 175-192. http://dx.doi.org/10.2166/nh.2021.104.

Gomes, D. J. C., Beltrão, N. E. S., Pereira, F. M., Reis, A. C. M., Pinheiro, A. M. P., & Silva, D. F. (2022). Estimativa de precipitação dos dados CHIRPS e GPCC em anos de extremos climáticos, Bacia Hidrográfica do rio Guamá-PA. *Revista Brasileira de Geografia Física*, *15*(3), 1583-1598. http://dx.doi.org/10.26848/rbgf.v15.3.p1583-1598.

Grimm, A. M. (2011). Interannual climate variability in South America: impacts on seasonal precipitation, extreme events, and possible effects of climate change. *Stochastic Environmental Research and Risk Assessment: Research Journal*, *25*(4), 537-554. http://dx.doi.org/10.1007/s00477-010-0420-1.

Grimm, A. M., Almeida, A. S., Beneti, C. A. A., & Leite, E. A. (2020). The combined effect of climate oscillations in producing extremes: the 2020 drought in southern Brazil. *Revista Brasileira de Recursos Hídricos*, *25*, e48. http://dx.doi.org/10.1590/2318-0331.252020200116.

Ilbay-Yupa, M., Lavado-Casimiro, W., Rau, P., Zubieta, R., & Castillón, F. (2021). Updating regionalization of precipitation in Ecuador. *Theoretical and Applied Climatology*, *143*(3-4), 1513-1528. http://dx.doi.org/10.1007/s00704-020-03476-x.

Kayano, M. T., & Capistrano, V. B. (2014). How the Atlantic multidecadal oscillation (AMO) modifies the ENSO influence on the South American rainfall. *International Journal of Climatology*, *34*(1), 162-178. https://doi.org/10.1002/joc.3674.

Kayano, M. T., Andreoli, R. V., & Souza, R. A. F. (2019). El Niño–Southern Oscillation related teleconnections over South America under distinct Atlantic Multidecadal Oscillation and Pacific Interdecadal Oscillation backgrounds: la Niña. *International Journal of Climatology*, *39*(3), 1359-1372. http://dx.doi.org/10.1002/joc.5886.

Kayano, M. T., Andreoli, R. V., & Souza, R. A. F. (2020). Pacific and Atlantic multidecadal variability relations to the El Niño events and their effects on the South American rainfall. *International Journal of Climatology*, *40*(4), 2183-2200. http://dx.doi.org/10.1002/joc.6326.

Kouakou, C., Paturel, J.-E., Satgé, F., Tramblay, Y., Defrance, D., & Rouché, N. (2023). Comparison of gridded precipitation estimates for regional hydrological modeling in West and Central Africa. *Journal of Hydrology. Regional Studies*, *47*, 101409. http://dx.doi.org/10.1016/j.ejrh.2023.101409.

Lima, C. E. S., Silva, M. V. M., Silveira, C. S., & Vasconcelos Junior, F. D. C. (2021). Wavelet transform for medium-range streamflows projections in national interconnected system. *Revista Brasileira de Ciências Ambientais*, *57*(1), 72-83. http://dx.doi.org/10.5327/z217694781048.

Liu, F., & Masago, Y. (2023). An analysis of the spatial heterogeneity of future climate change impacts in support of cross-sectoral adaptation strategies in Japan. *Climate Risk Management*, *41*, 100528. http://dx.doi.org/10.1016/j.crm.2023.100528.

Lucas, E. W. M., Sousa, F. A. S., Silva, F. D. S., Rocha Júnior, R. L., Pinto, D. D. C., & Silva, V. P. R. (2021). Trends in climate extreme indices assessed in the Xingu river basin - Brazilian Amazon. *Weather and Climate Extremes*, *31*, 100306. https://doi.org/10.1016/j.wace.2021.100306.

Marengo, J. A., & Espinoza, J. C. (2016). Extreme seasonal droughts and floods in Amazonia: causes, trends and impacts. *International Journal of Climatology*, *36*(3), 1033-1050. http://dx.doi.org/10.1002/joc.4420.

Marengo, J. A., Alves, L. M., Alvala, R. C. S., Cunha, A. P., Brito, S., & Moraes, O. L. L. (2018). Climatic characteristics of the 2010-2016 drought in the semiarid Northeast Brazil region. *Anais da Academia Brasileira de Ciências*, *90*(2, Suppl. 1), 1973-1985. http://dx.doi.org/10.1590/0001-3765201720170206.

Marengo, J. A., Galdos, M. V., Challinor, A., Cunha, A. P., Marin, F. R., Vianna, M. S., Alvala, R. C. S., Alves, L. M., Moraes, O. L., & Bender, F. (2022). Drought in Northeast Brazil: a review of agricultural and policy adaptation options for food security. *Climate Resilience and Sustainability*, *1*(1), e17. http://dx.doi.org/10.1002/cli2.17.

Marengo, J. A., Torres, R. R., & Alves, L. M. (2017). Drought in Northeast Brazil: past, present, and future. *Theoretical and Applied Climatology*, *129*(3-4), 1189-1200. http://dx.doi.org/10.1007/s00704-016-1840-8.

McKee, T. B., Doesken, N. J., & Kleist, J. (1993) The relationship of drought frequency and duration to time scales. In *8th Conference on Applied Climatology* (pp. 179-184), Anaheim. Retrieved in 2024, May 5, from https://www.droughtmanagement.info/literature/AMS_Relationship_Drought_Frequency_Duration_Time_Scales_1993.pdf

Merino, A., Fernández-Vaquero, M., López, L., Fernández-González, S., Hermida, L., Sánchez, J. L., García-Ortega, E., & Gascón, E. (2015). Large-scale patterns of daily precipitation extremes on the Iberian Peninsula. *International Journal of Climatology*, *36*(11), 3873-3891. http://dx.doi.org/10.1002/joc.4601 .

Pezzi, L. P., Quadro, M. F. L., Souza, E. B., Miller, A. J., Rao, V. B., Rosa, E. B., Santini, M. F., Bender, A., Souza, R. B., Cabrera, M. J., Parise, C. K., Carvalho, J. T., Lima, L. S., Quadros, M. R. L., Nehme, D. M., & António, J. F. (2023). Oceanic SACZ produces an abnormally wet 2021/2022 rainy season in South America. *Scientific Reports*, *13*(1), http://dx.doi.org/10.1038/s41598-023-28803-w.

Pontes Filho, J. D., Souza Filho, F. A., Martins, E. S. P. R., & Studart, T. M. C. (2020). Copula-based multivariate frequency analysis of the 2012–2018 drought in Northeast Brazil. *Water*, *12*(3), 834. http://dx.doi.org/10.3390/w12030834.

Reboita, M. S., Gan, M. A., Rocha, R. P., & Ambrizzi, T. (2010). Regimes de precipitação na América do Sul: uma revisão bibliográfica. *Revista Brasileira de Meteorologia*, *25*(2), 185-204. http://dx.doi.org/10.1590/s0102-77862010000200004.

Reboita, M. S., Ambrizzi, T., Crespo, N. M., Dutra, L. M. M., Ferreira, G. W. S., Rehbein, A., Drumond, A., Rocha, R. P., &

Souza, C. A. (2021). Impacts of teleconnection patterns on South America climate. *Annals of the New York Academy of Sciences*, *1504*(1), 116-153. http://dx.doi.org/10.1111/nyas.14592.

Ribeiro Neto, G. G., Melsen, L. A., Martins, E. S. P. R., Walker, D. W., & van Oel, P. R. (2022). Drought Cycle Analysis to evaluate the influence of a dense network of small reservoirs on drought evolution. *Water Resources Research*, *58*(1), http://dx.doi.org/10.1029/2021wr030799.

Rocha, R. V., Souza Filho, F. A., & Silva, S. M. O. (2019). Análise da relação entre a precipitação média do reservatório Orós, Brasil - Ceará, e os índices PDO e AMO Através da análise de changepoints e transformada de ondeletas. *Revista Brasileira de Meteorologia*, *34*(1), 139-149. http://dx.doi.org/10.1590/0102-77863340034.

Rocha, R. V., & Souza Filho, F. A. (2020). Mapping abrupt streamflow shift in an abrupt climate shift through multiple change point methodologies: Brazil case study. *Journal Des Sciences Hydrologiques*, *65*(16), 2783-2796. http://dx.doi.org/10.1080/02626667.2020.1843657 .

Roesch, A., & Schmidbauer, H. (2018). *Wavelet comp: computational wavelet analysis. R package version 1.1*. Vienna: R Foundation for Statistical Computing. Retrieved in 2024, May 5, from https://CRAN.R-project.org/package=WaveletComp

Roushangar, K., Moghaddas, M., Ghasempour, R., & Alizadeh, F. (2021). Evaluation of spatial-temporal characteristics of precipitation using discrete maximal overlap wavelet transform and spatial clustering tools. *Hydrology Research*, *52*(2), 414-430. http://dx.doi.org/10.2166/nh.2021.141.

Santos, D. C., Santos, C. A. G., Brasil Neto, R. M., Silva, R. M., & Santos, C. A. C. (2023). Precipitation variability using GPCC data and its relationship with atmospheric teleconnections in Northeast Brazil. *Climate Dynamics*, *61*(11-12), 5035-5048. http://dx.doi.org/10.1007/s00382-023-06838-z.

Schneider, U., Hänsel, S., Finger, P., Rustemeier, E., & Ziese, M. (2022). *GPCC full data monthly version 2022 at 1.0°: Monthly land-surface precipitation from rain-gauges built on GTS-based and historic data*. Offenbach am Main: Global Precipitation Climatology Centre (GPCC). http://dx.doi.org/10.5676/DWD_GPCC/FD_M_V2022_100.

Sebaziga, J. N., Twahirwa, A., Kazora, J., Rusanganwa, F., Mbati, M. M., Higiro, S., Guhirwa, S., Nyandwi, J. C., & Niyitegeka, J. M. V. (2023). Spatial and temporal analysis of rainfall variability and trends for improved climate risk management in Kayonza District, eastern Rwanda. *Advances in Meteorology*, *2023*, 1-17. http://dx.doi.org/10.1155/2023/5372701.

Song, L., Xu, C., Long, Y., Lei, X., Suo, N., & Cao, L. (2022). Performance of seven gridded precipitation products over arid Central Asia and subregions. *Remote Sensing*, *14*(23), 6039. http://dx.doi.org/10.3390/rs14236039.

Staal, A., Tuinenburg, O. A., Bosmans, J. H. C., Holmgren, M., van Nes, E. H., Scheffer, M., Zemp, D. C., & Dekker, S. C. (2018). Forest-rainfall cascades buffer against drought across the Amazon. *Nature Climate Change*, *8*(6), 539-543. http://dx.doi.org/10.1038/s41558-018-0177-y.

Tibebe, D., Degefu, M. A., Bewket, W., Teferi, E., O'Donnell, G., & Walsh, C. (2023). Homogenous climatic regions for targeting green water management technologies in the Abbay basin, Ethiopia. *Climate*, *11*(10), 212. http://dx.doi.org/10.3390/cli11100212.

Torrence, C., & Compo, G. P. (1998). A practical guide to wavelet analysis. *Bulletin of the American Meteorological Society*, *79*(1), 61-78. http://dx.doi.org/10.1175/1520-0477(1998)079<0061:apgtwa>2.0.co;2.

Xavier, A. C., Scanlon, B. R., King, C. W., & Alves, A. I. (2022). New improved Brazilian daily weather gridded data (1961–2020). *International Journal of Climatology*, *42*(16), 8390-8404. http://dx.doi.org/10.1002/joc.7731.

Authors contributions

Carlos Eduardo Sousa Lima: Conceptualization, data curation, formal analysis, investigation, methodology, software, validation, visualization, writing – original draft, writing - review & editing.

Francisco de Assis Souza Filho: Conceptualization, methodology, supervision, validation, writing - review & editing.

Renan Vieira Rocha: Supervision, validation, writing - review & editing.

Editor-in-Chief: Adilson Pinheiro

Associated Editor: Carlos Henrique Ribeiro Lima

SUPPLEMENTARY DATA

Supplementary material accompanies this paper.

Supplementary Material A. Centroide dos Agrupamentos e Índice Climático ONI.

This material is available as part of the online article from https://doi.org/10.1590/2318-0331.302520240102